Simulation of Heat Transfer in Building -Integrated Photovoltaics (BIPV) Using Computation Fluid Dynamics

Yong You[1], Qiuhua (Lisa) Duan[1,*]
[1] Department of Civil, Construction and Environmental Engineering, University of Alabama, Tuscaloosa, USA

*qduan@ua.edu

Abstract

Building-Integrated Photovoltaics (BIPV) are gaining prominence as a sustainable solution for energy generation and architectural integration. However, the thermal performance of BIPV systems significantly influences their electrical efficiency and structural durability. This study leverages Computational Fluid Dynamics (CFD) to simulate the heat transfer mechanisms in BIPV systems, providing insights into optimizing their thermal behavior under varying environmental and operational conditions.

1. Introduction

Since PV windows absorb a significant portion of solar radiation, they impose complex effects on the indoor thermal environment, which in turn influences occupants' thermal comfort. Therefore, it is essential to investigate the indoor environmental performance, particularly the thermal conditions of buildings equipped with PV glazing systems.

2. Methods

2.1 Physical model

Fig. 1 illustrates the physical model used in this study. The glazing module is installed on the south wall. The clear glazing consists of two clear glass layers. The outer surface of the PV window is a clear glass layer, and below that, in order, is EVA layer, CdTe cell, EVA layer and finally clear glass. Four transmittance levels of the CdTe cell (15%, 20%, 25% and 30%) are considered to represent different coverage ratios of the CdTe cell area.

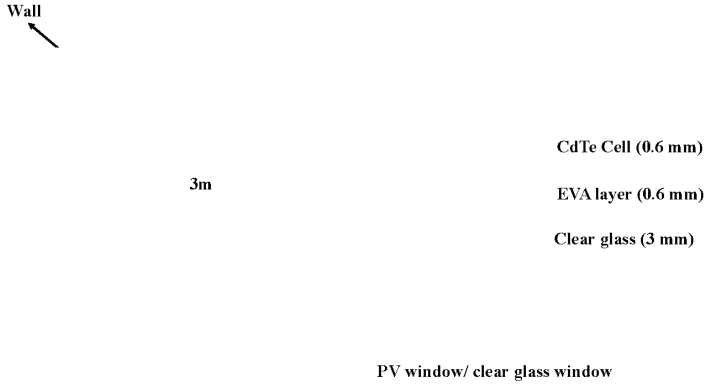

Fig. 1 Schematic of the room and glazing module.

The physical and optical properties of the PV module are summarized in Table 1 (Radwan and Ahmed, 2012; Virtuani et al., 2010; Strauss, 1977) and Table 2 (Krauter, 1996).

Table 1. Physical properties for the materials used.

Component	Thickness	Density	Specific heat	Thermal conductivity

https://doi.org/10.52202/083252-0012

	(mm)	$(kg/m3)$	$(J/(kg\cdot K))$	$(W/(m\cdot K))$
Clear glass	3	3000	691	2
EVA	0.6	960	2090	0.35
CdTe cell	0.6	5850	24685	7.5

Table 2. Optical properties for the material used.

Component	Parameter	Value
Clear glass	Emissivity	0.88
	Absorption coefficient	26 for $\lambda < 4.25\mu m$ 1100 for $\lambda > 4.25\mu m$
	Refractive index	1.526
EVA	Refractive index	1.45
	Transmissivity	0.9
CdTe cell	Absorptivity	0.793

2.2 Thermal, turbulent and optical modeling

2.2.1 Thermal and turbulent modeling

Considering the above assumptions, the governing equations for the heat transfer in this problem are as follows.

Mass Conservation:

$$\frac{\partial \rho}{\partial t} + \nabla \bullet (\rho u) = S_m \#(1)$$

Momentum Conservation:

$$\frac{\partial (\rho u)}{\partial t} + \nabla \bullet (\rho u u) = -\nabla \bullet (\bar{\bar{\tau}}) + \rho g + F \#(2)$$

Energy Conservation:

$$\frac{\partial \rho E}{\partial t} + \nabla \bullet (u(\rho E + p)) = -\nabla \bullet \left(\sum_j h_j J_j\right) + S_h \#(3)$$

Realizable k-e Transport Equation:

$$\frac{\partial (\rho k)}{\partial t} + \frac{\partial \left(\rho k u_j\right)}{\partial x_j} = \frac{\partial}{\partial x_j}\left[\left(\mu + \frac{\mu_t}{\sigma_k}\right)\frac{\partial k}{\partial x_j}\right] + G_k + G_b - \rho\varepsilon - Y_M + S_k \#(4)$$

$$\frac{\partial (\rho \varepsilon)}{\partial t} + \frac{\partial \left(\rho \varepsilon u_j\right)}{\partial x_j} = \frac{\partial}{\partial x_j}\left[\left(\mu + \frac{\mu_t}{\sigma_\varepsilon}\right)\frac{\partial \varepsilon}{\partial x_j}\right] + \rho C_1 S\varepsilon - \rho C_2 \frac{\varepsilon^2}{k+\sqrt{\nu\varepsilon}} + C_{1\varepsilon}\frac{\varepsilon}{k}C_{3\varepsilon}G_b + S_\varepsilon \#(5)$$

2.2.2 Electrical power modeling

The solar cell's electrical energy efficiency is calculated using Eq.(6) (Zaghloul et al., 2021;) $(6)(6)(6)(6)(6)(6)$the cell temperature obtained from simulation results. The electrical CdTe PV cell output power is then calculated using Eq.(7) (7) (Abo-Zahhad et al., 2018)

$$\eta_{cell} = \eta_{ref}\left(1 + \beta_{rel}\left(T_{cell} - T_{ref}\right)\right) \#(6)$$

$$P_{el} = \eta_{cell} E_t \tau_{o-pv} \alpha_{cell} A_{cell} \#(7)$$

2.2.3 Optical modeling

In the present study, for solving the RTE, the 'Discrete Ordinate' (DO) radiation model is employe. The DO radiation model for the spectral intensity at position in the direction is written as:

$$\nabla \cdot \left(I_\lambda(r,s)s\right) + \left(\sigma_\lambda + \sigma_s\right)I_\lambda(r,s) = \sigma_\lambda n^2 I_{b\lambda} + \frac{\sigma_s}{4\pi}\int_0^{4\pi} I_\lambda(r,s)\Phi\left(s \cdot s'\right)d\Omega' \#(8)$$

https://doi.org/10.52202/083252-0012

2.2.4 Boundary conditions

The boundary of the outer surface of the clear glass is set as a combined convection and radiation boundary conditions. The external radiation temperature is set equal to the sky temperature, which is calculated using Eq. (9).

$$T_{sky} = 0.0552 T_{amb}^{1.5} \#(9)$$

The convective heat transfer coefficient of ambient air flowing over the outer surface of the PV module is calculated based on Eq. (10).

$$h = h_{wind} = 5.7 + 3.8 V_{wind} \#(10)$$

3. Results and Discussion

3.1 Thermal performance

Fig. 2 presents the hourly boundary conditions of Tuscaloosa city, extracted from the NSRDB database, including global horizontal irradiance (GHI), direct normal irradiance (DHI), and ambient temperature for typical days in winter (a), summer (b), and the transition season (c).

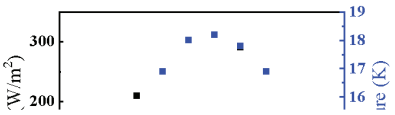

Fig. 2 Hourly boundary conditions from the NSRDB, including global horizontal irradiance, direct normal irradiance, and ambient temperature for three typical days: winter (a), summer (b), and transition season (c).

To evaluate the indoor thermal environment, a horizontal reference plane was established at a height of 0.6 m above the floor. A total of 108 uniformly distributed sampling points were arranged to monitor air temperature, and the standard deviation of the temperatures at these points was used to represent the indoor temperature non-uniformity (σ).

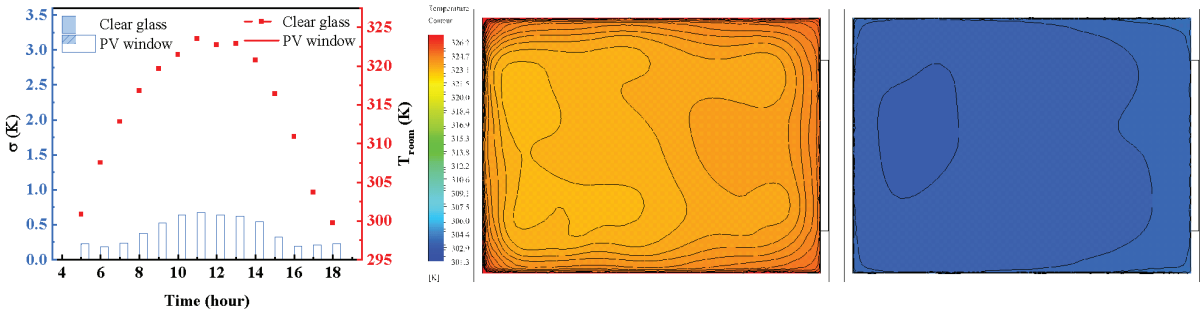

Fig. 3 illustrates the diurnal variations of indoor air average temperature and temperature non-uniformity under typical summer conditions with clear glass and PV windows. The results indicate that the PV window significantly reduces the indoor average temperature, with a decrease of more than 20 K at 11:00. Moreover, the PV window remarkably mitigates thermal non-uniformity (σ).

https://doi.org/10.52202/083252-0012

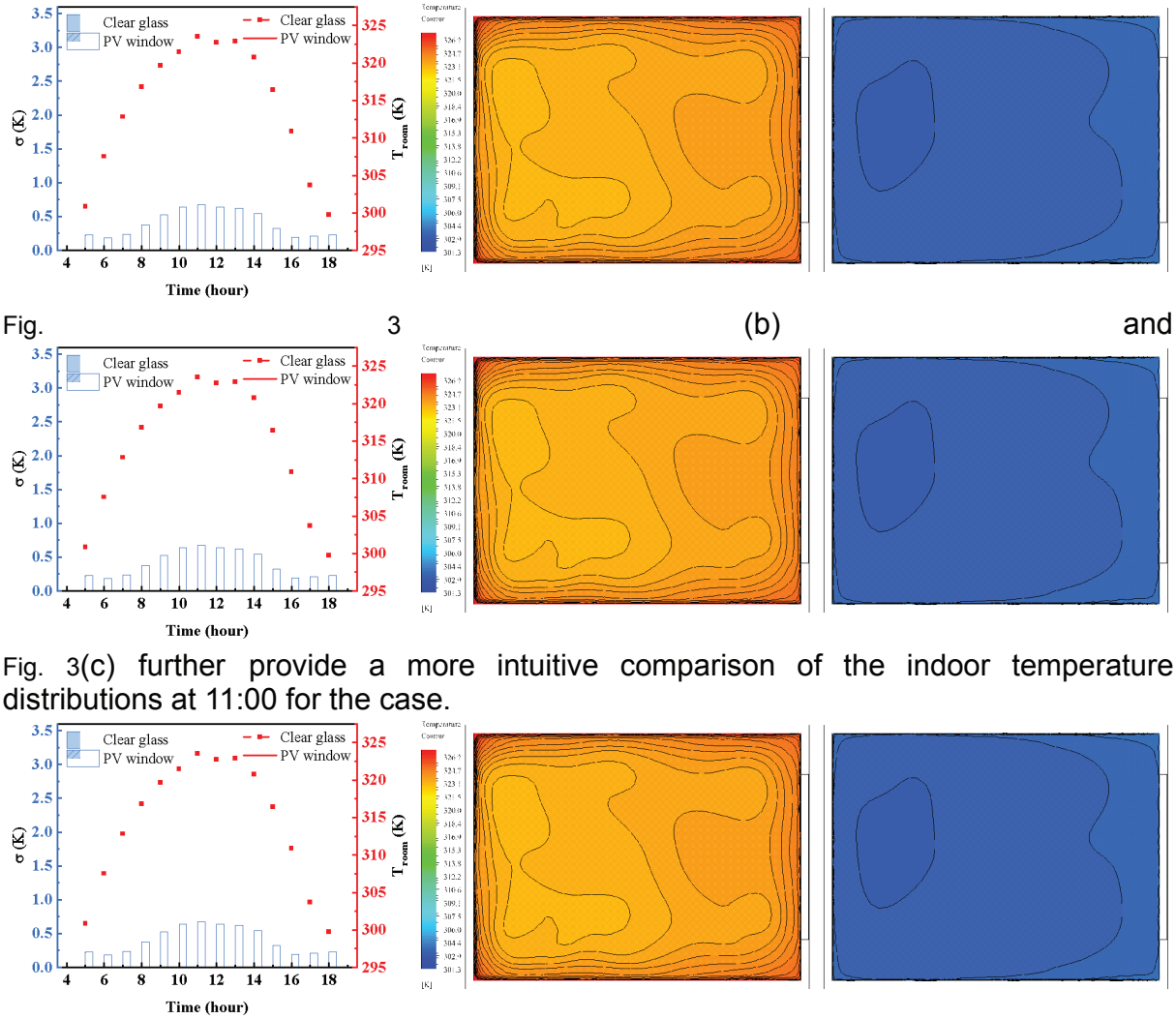

Fig. 3 (b) and Fig. 3(c) further provide a more intuitive comparison of the indoor temperature distributions at 11:00 for the case.

Fig. 3 Indoor average temperature and temperature non-uniformity on a typical summer day (a), and indoor temperature distribution at 11:00 am (b: clear glass, c: PV window).

Like the summer scenario, the PV window reduces both the indoor average temperature and thermal non-uniformity compared with clear glass. However, the reductions are less pronounced due to the lower ambient thermal loads in the transitional season and winter.

3.2 Electrical performance

As shown in Fig. 4 (a), the electrical efficiency of the PV is higher in the early morning and late afternoon, while it reaches the lowest value around noon. This phenomenon is mainly attributed to the temperature effect of PV modules: elevated module temperatures at midday significantly reduce efficiency. Seasonal comparisons indicate that the electrical efficiency is highest in winter, followed by the transition season, and lowest in summer. Fig. 4 (b) shows that the electrical output power is highest in summer, moderate in the transition season, and lowest in winter, with the shortest duration of high-power generation. Overall, PV windows demonstrate higher energy conversion efficiency in winter but achieve the smallest electricity generation due to weaker

https://doi.org/10.52202/083252-0012

irradiance, while in summer, despite lower efficiency, the stronger irradiance and longer sunshine duration lead to significantly higher power generation, with the transition season falling in between.

(a) (b)

Fig. 4 Variation of PV cell efficiency (a) and power output (b) on typical meteorological days

4. Conclusions

- PV windows significantly reduced indoor average temperature and thermal non-uniformity compared with clear glazing.
- PV windows exhibited the highest conversion efficiency in winter but achieved the greatest electricity generation in summer due to stronger irradiance and longer sunshine duration, with the transitional season falling in between.
- PV windows provide a dual advantage of improved indoor comfort and renewable electricity generation, with particularly high potential in hot climates.

References

[1] Abo-Zahhad E M , Ookawara S , Radwan A ,et al.Thermal and structure analyses of high concentrator solar cell under confined jet impingement cooling[J].Energy Conversion and Management, 2018,176(NOV.):39-54.DOI:10.1016/j.enconman.2018.09.005.
[2] Zaghloul H , Emam M , Abdelrahman M A ,et al.Optimization and parametric analysis of a multi-junction high-concentrator PV cell combined with a straight fins heat sink[J].Energy Conversion and Management, 2021,243(S1):114382.DOI:10.1016/j.enconman.2021.114382.
[3] Krauter S , Hanitsch R .Actual optical and thermal performance of PV-modules[C]//IEEE First World Conference on Photovoltaic Energy Conversion, Conference Record of the Twenty Fourth IEEE Photovoltaic Specialists Conference.IEEE, 1996.DOI:10.1109/WCPEC.1994.520063.
[4] Strauss A .The physical properties of cadmium telluride[J]. 1977.DOI:10.1051/RPHYSAP:01977001202016700.
[5] Virtuani A , Pavanello D , Friesen G .Overview of Temperature Coefficients of Different Thin Film Photovoltaic Technologies[C]//25th EU-PVSEC.2010.DOI:10.4229/25thEUPVSEC2010-4AV.3.83.
[6] Radwan A , Ahmed M .The influence of microchannel heat sink configurations on the performance of low concentrator photovoltaic systems[J].Applied Energy, 2017, 206(nov.15):594-611.DOI:10.1016/j.apenergy.2017.08.202.